Supporting Information for

Helicity Adaptation within a Quadruply Stranded Helicate by Encapsulation

Qi Lin,[a] Lei Gao,[a] Brice Kauffmann,[b] Jiajia Zhang,[a] Chunmiao Ma,[a] Dan Luo[a] and

Quan Gan*[ac]

[a]Hubei Key Laboratory of Bioinorganic Chemistry & Materia Medica, School of Chemistry and Chemical Engineering, Huazhong University of Science and Technology, Wuhan 430074, P. R. China

[b]Université de Bordeaux, CNRS, INSERM, IECB–UMS3033–US001, Institut Européen de Chimie et Biologie, 2 rue Robert Escarpit, 33600 Pessac, France

[c]Shenzhen Institute of Huazhong University of Science & Technology, Shenzhen 518000, P. R. China

Correspondence and requests for materials should be addressed to Quan Gan (ganquan@hust.edu.cn).

Table of contents

1 Experimental procedures 3

1.1 General methods 3

1.2 Synthesis of helicate **1** 3

2 Solution spectroscopic analysis of helicates 9

2.1 ^{1}H NMR spectroscopy of **1**•$(NO_3)_4$ with different propotions of DMSO-d_6 9

2.2 Variable temperature ^{1}H NMR spectroscopy of **1**•$(BF_4)_4$ 10

2.3 Formation of the host-guest complex **2** 10

2.4 Variable temperature ^{1}H NMR titration complex **2** 11

3 X-Ray Crystallography 14

4 Circular dichroism studies 21

5 Volume calculations 22

6 NMR spectra 23

7 References 25

1 Experimental procedures

1.1 General methods

All chemicals and solvents were purchased from commercial suppliers and were used without further purification unless otherwise specified. Tetrahydrofuran (THF) was distilled over sodium/benzophenone and dichloromethane (DCM) and triethylamine (Et_3N) was distilled over CaH_2 prior to use. Column chromatography was carried out on Merck GEDURAN Si60 (40-63 µm). High-resolution electrospray ionization mass spectrometry (ESI-MS) was performed on a micro TOF II instrument featuring a Z spray source with electrospray ionization and modular LockSpray interface.

NMR spectra were recorded on Bruker AVANCE 600 (600 MHz), and Bruker AVANCE 400 (400 MHz) spectrometers. The solvent signals were assigned by Fulmer et al.[S1] All chemical shifts (δ) are quoted in ppm and coupling constants (*J*) are expressed in Hertz (Hz). The following abbreviations are used for convenience in reporting the multiplicity for NMR resonances: s = singlet, d = doublet, t = triplet, and m = multiplet. Data processing was performed with Topspin 2.0 software. Assignment of all ^1H and ^{13}C resonances was achieved using standard 2D NMR techniques: ^1H-^1H COSY, ^1H-^1H NOESY, and ^1H-^{13}C HSQC.

1.2 Synthesis of helicate **1**

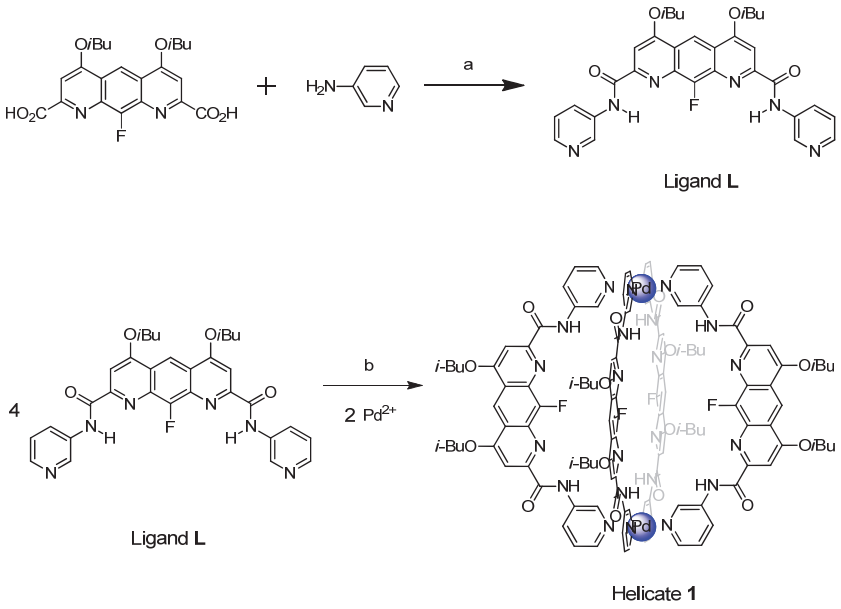

Scheme S1. Synthesis of helicate **1**. a) oxalyl chloride, DCM, rt, 2h, then TEA, DCM, rt, 2h; b) DCM, CH_3CN, 55 °C, 6 h.

Ligand **L**. To a solution of anthracene diacid[S2] (0.50 g, 1.16 mmol) in anhydrous DCM (10 ml) under nitrogen was added oxalyl chloride (0.99 mL, 10.0 eq.) at 0°C. The reaction was then stirred for 3 hours at room temperature. Reactions were monitored by ^{1}H NMR. When the anthracene diacid all converted into acid chloride, Solvent was removed under reduced pressure to yield a yellow solid. This solid was then redissolved in anhydrous DCM and slowly added at 0°C to a solution of 3-aminopyridine (0.33 g, 3.48 mmol) and *N*,*N*-diisopropylethylamine (0.99 ml, 5.81 mmol) in anhydrous DCM under nitrogen atmosphere. The resulting mixture was stirred at room temperature for 12 h. Solvents were evaporated and the crude material purified by flashchromatography with DCM/MeOH (90:10) to yield the pure compound as a yellow solid (0.58 g, 85%). ^{1}H NMR ($CDCl_3$, 400 MHz): δ 10.44 (s, 2H), 9.07 (s, 1H), 9.03 (d, J = 2.12 Hz, 2H), 8.46 (d, J = 4.24 Hz, 2H), 8.41 (d, J = 8.24 Hz, 2H), 7.77 (s, 2H), 7.40 (dd, J = 8.12, 4.76 Hz, 2H), 4.22 (d, J = 6.36 Hz, 4H), 2.40 (m, 2H), 1.21 (d, J = 6.68 Hz, 12H). ^{13}C NMR ($CDCl_3$, 100 MHz): δ 164.0, 162.4, 154.5, 152.9, 145.8, 141.8, 135.3, 135.2, 134.5, 127.0, 123.9, 122.3, 111.7, 111.6, 97.4, 77.5, 77.2, 76.8, 75.8, 28.4, 19.2. ESI-HRMS: m/z calcd for $[M+H]^+$ 583.2469, found 583.2401. Elemental analysis (%): calculated for $C_{32}H_{31}FN_6O_4$, C 65.97, H 5.36, N 14.42; found, C 65.63, H 5.27, N 14.34.

Synthesis of helicate **1**•$(NO_3)_4$. $Pd(NO_3)_2$ (2.1 mg) was dissolved in CH_3CN (0.5 ml), and then to a solution of ligand **L** (10 mg) in $CHCl_3$ (5.0 ml) was added the above $Pd(NO_3)_2$ solution. The mixture was stirred for 6 h at 55°C. Hexane (20 mL) was added into the reaction mixture and the product as pale yellow precipitate was collected by vacuum filtration (9.94 mg, 83%). ^{1}H NMR ($CDCl_3$/CD_3CN 10:1, 400 MHz): δ 11.03 (s, 2H), 9.12 (s, 2H), 9.07 (d, J = 8.64 Hz, 2H), 8.92 (s, 1H), 8.77 (d, J = 6.04 Hz, 2H), 7.56 (s, 2H), 7.45 (t, J = 5.76 Hz, 2H), 4.06 (d, J = 6.20 Hz, 4H), 2.26 (m, 2H), 1.08 (d, J = 6.52 Hz, 12H). ESI-HRMS: m/z calcd for $[\mathbf{1}\bullet(NO_3)_2]^{2+}$ 1333.3724, found 1333.3937. Elemental analysis (%): calculated for $C_{128}H_{124}F_4N_{28}O_{28}Pd_2$, C 55.08, H 4.48, N 14.05; found, C 55.01, H 4.22, N 14.12.

Synthesis of helicate **1**•$(BF_4)_4$. $Pd(CH_3CN)_4(BF_4)_2$ (4 mg) was dissolved in CH_3CN (0.5 ml), and then to a solution of ligand **L** (10 mg) in $CHCl_3$ (5.0 ml) was added the above $Pd(BF_4)_2$ solution. The mixture was stirred for 6 h at 55°C. Hexane (20 mL) was added into the the reaction mixture and the product as pale yellow precipitate was collected by vacuum filtration (11.16 mg, 90%). ^{1}H NMR ($CDCl_3$/CD_3CN 10:1, 400 MHz): δ 10.65 (s, 2H), 9.09 (d, J = 6.92 Hz, 2H), 9.00 (s, 2H), 8.91 (s, 1H), 8.51 (d, J = 4.68 Hz, 2H), 7.54 (s, 2H), 7.44 (dd, J = 6.64,4.72 Hz, 2H), 4.05 (d, J = 4.88 Hz, 4H), 2.25(m, 2H), 1.08 (d, J = 5.20 Hz, 12H). ^{13}C NMR ($CDCl_3$/CD_3CN 10:1, 100 MHz) δ 172.7, 163.7, 163.3, 152.7, 146.5, 143.5, 137.7, 135.4, 135.3, 131.2, 126.6, 122.1, 116.5, 97.6, 77.5, 77.2, 76.8, 75.4, 28.0, 18.8, 1.8, 1.6, 1.4, 1.2, 1.0. ESI-HRMS: m/z calcd for $[\mathbf{1}\bullet(BF_4)_2]^{2+}$ 1358.3887, found 1358.3864. Elemental analysis (%): calculated for $C_{128}H_{124}B_4F_{20}N_{24}O_{16}Pd_2$, C 53.19, H 4.32, N 11.63; found, C 53.06, H 4.15, N 11.42.

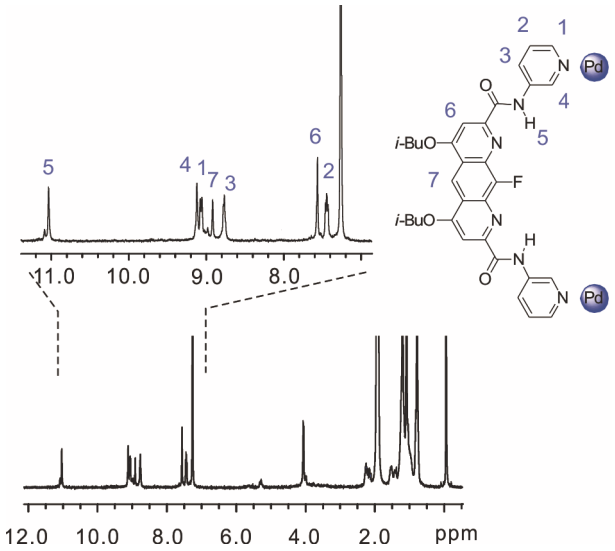

Figure S1. ^{1}H NMR spectrum ($CDCl_3$:CD_3CN = 10:1, 400 MHz, 298 K) of **1**•$(NO_3)_4$ with assignment of signals. It shows two sets of peacks for the ligand's each proton environment, representing the formation of two isomers.

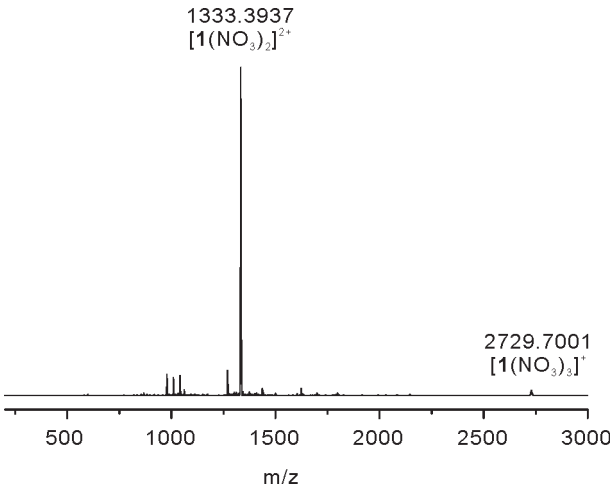

Figure S2. Traces of the high-resolution ESI-MS of **1**•$(NO_3)_4$ corresponding to 1+ and 2+ signals.

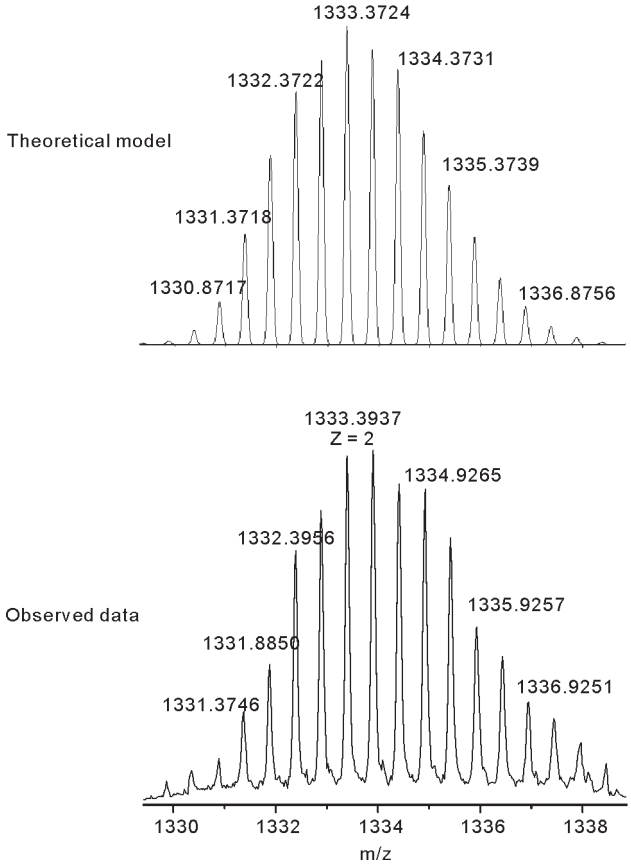

Figure S3. High-resolution ESI-MS data for the +2 peaks of **1**•$(NO_3)_4$.

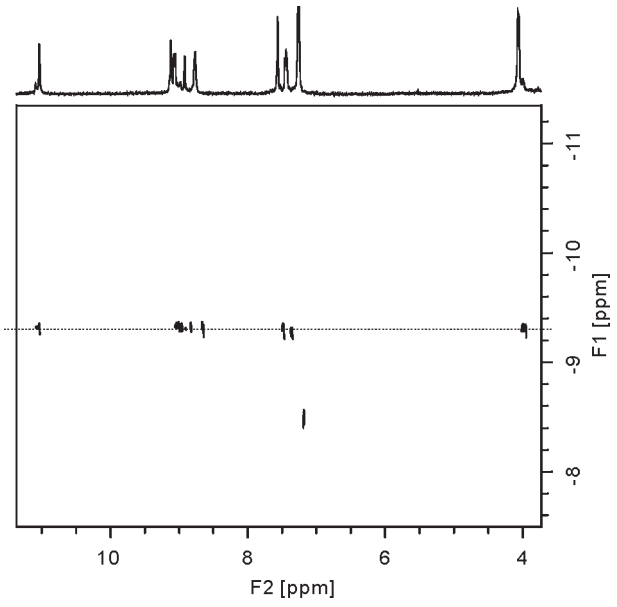

Figure S4. DOSY spectra ($CDCl_3$:CD_3CN = 10:1, 400 MHz, 298 K) of **1**•$(NO_3)_4$.

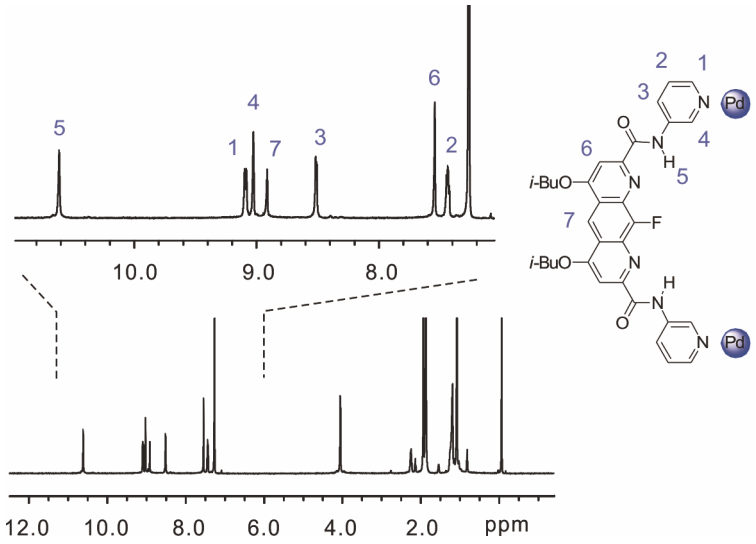

Figure S5. ^{1}H NMR spectrum ($CDCl_3$:CD_3CN = 10:1, 400 MHz, 298 K) of **1**•$(BF_4)_4$ with assignment of signals.

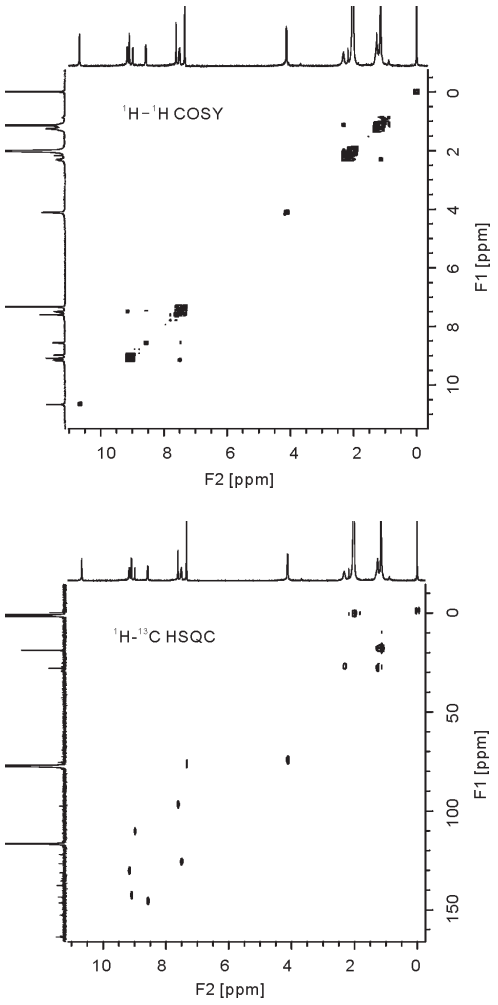

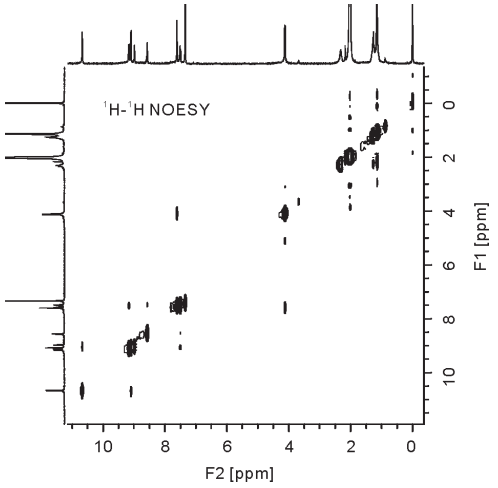

Figure S6. ^{1}H-^{1}H COSY, ^{1}H-^{13}C HSQC, and ^{1}H-^{1}H NOESY spectra ($CDCl_3$:CD_3CN = 10:1, 400 MHz, 298 K) of **1**•$(BF_4)_4$.

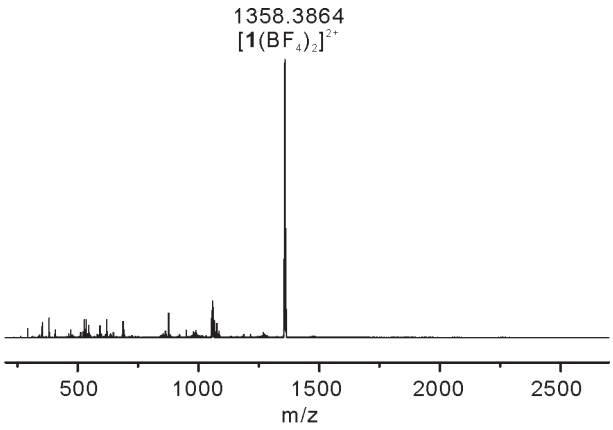

Figure S7. Traces of the high-resolution ESI-MS of **1**•$(BF_4)_4$ corresponding to 2+ signals.

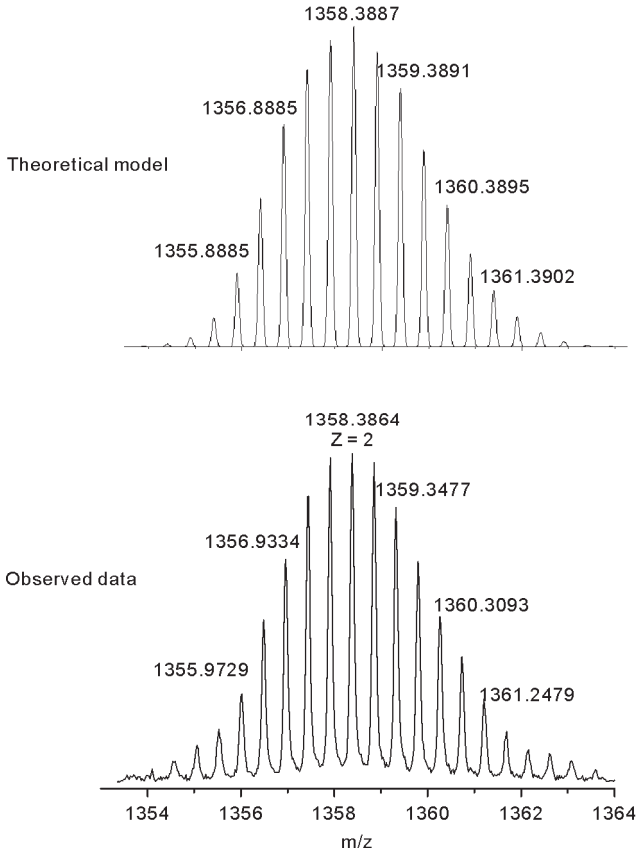

Figure S8. High-resolution ESI-MS data for the +2 peaks of **1**•$(BF_4)_4$.

2 Solution spectroscopic analysis of helicates

2.1 ^{1}H NMR spectroscopy of **1**•$(NO_3)_4$ with different propotions of DMSO-d_6

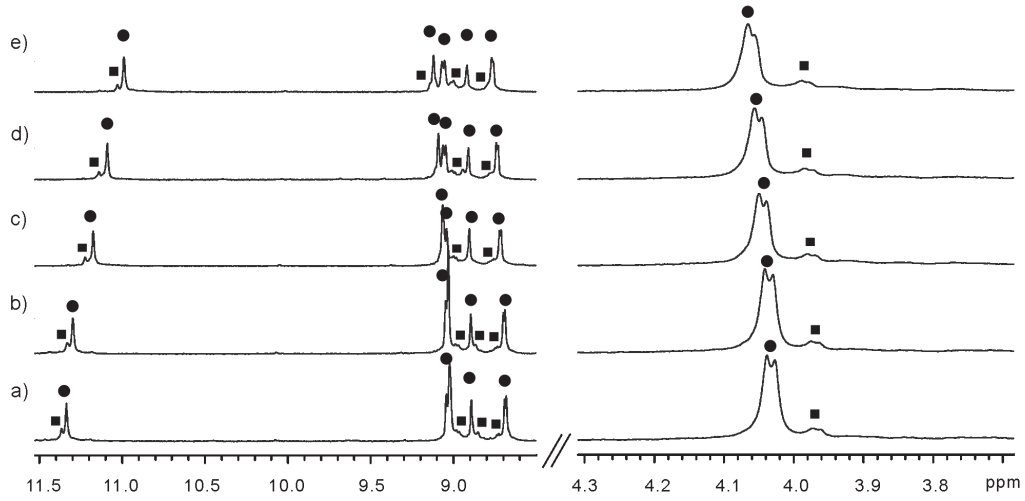

Figure S9. ^{1}H NMR spectra (400 MHz) of **1**•$(NO_3)_4$ (1 mM) in $CDCl_3$:CD_3CN:DMSO-d_6 (vol/vol/vol) (a) 10:1:0; (b) 10:1:1; (c) 10:1:4; (d) 10:1:6; (e) 10:1:10. The black circles and squares indicate different isomers.

2.2 Variable temperature ^{1}H NMR spectroscopy of **1**•$(BF_4)_4$

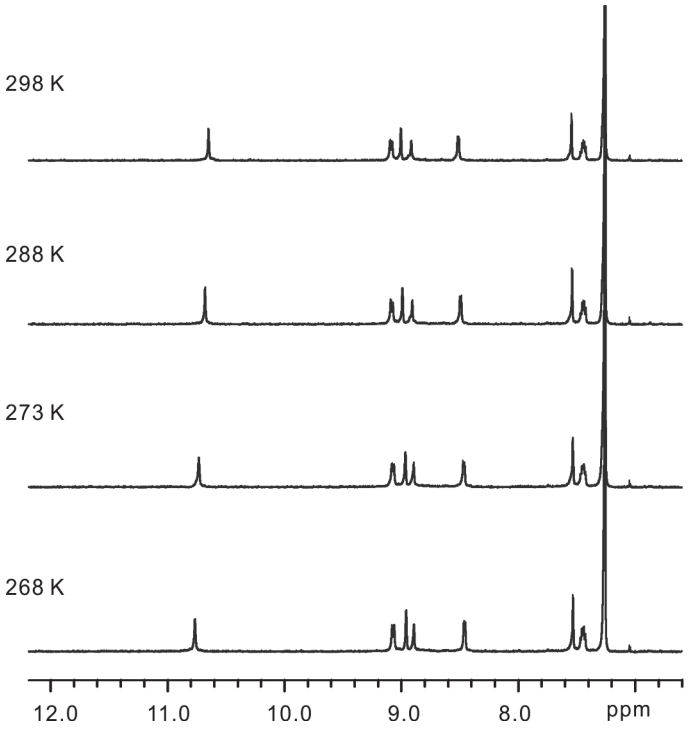

Figure S10. Temperature-dependent ^{1}H NMR spectra (400 MHz) of **1**•$(BF_4)_4$ (1 mM) in $CDCl_3$:CD_3CN = 10:1.

2.3 Formation of the host-guest complex **2**

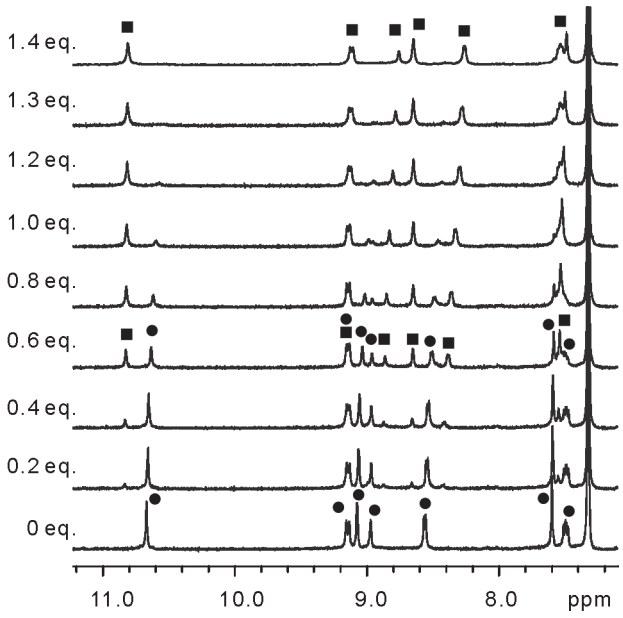

Figure S11. ^{1}H NMR titration of $B_{12}F_{12}^{2-}$ anion into a solution of **1**•$(BF_4)_4$ (0.5 mM) in $CDCl_3$:CD_3CN = 10:1 at 298 K. The black squares denote the 1:1 complex **2** whereas black circles denote the free helicate **1**. $Ka = 1.1 \times 10^4$ L mol^{-1}.

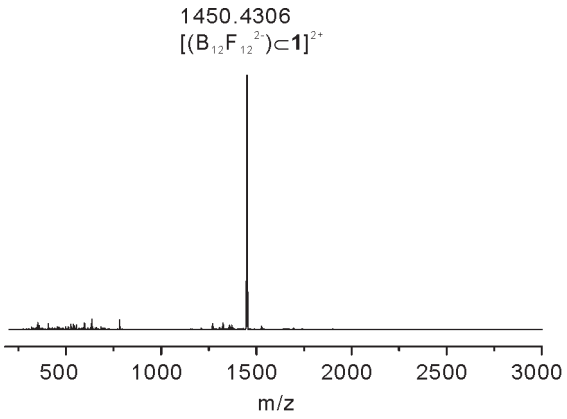

Figure S12. Traces of the high-resolution ESI-MS of complex **2** corresponding to +2 charged signals.

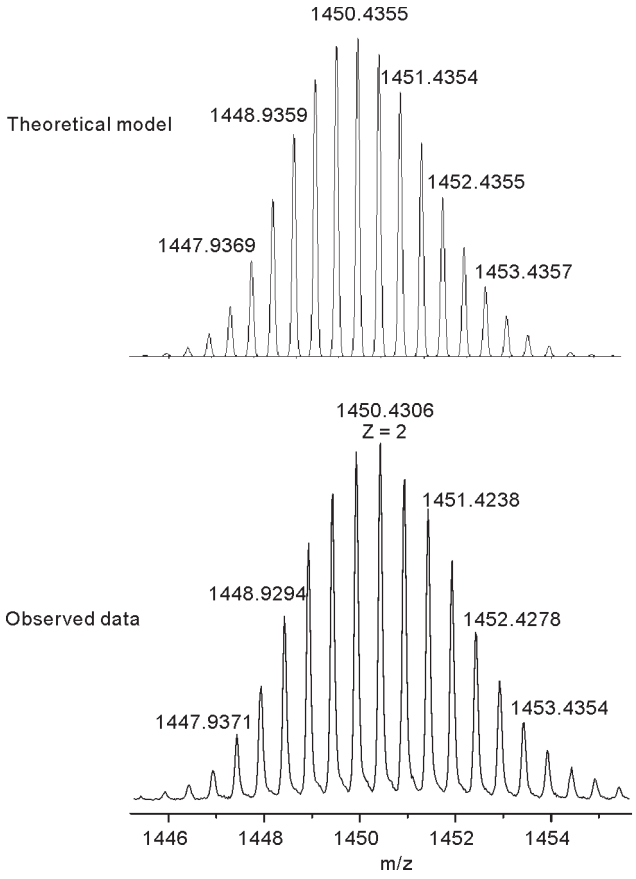

Figure S13. High-resolution ESI-MS data for the +2 peaks of complex **2**.

2.4 Variable temperature ^{1}H NMR titration complex **2**

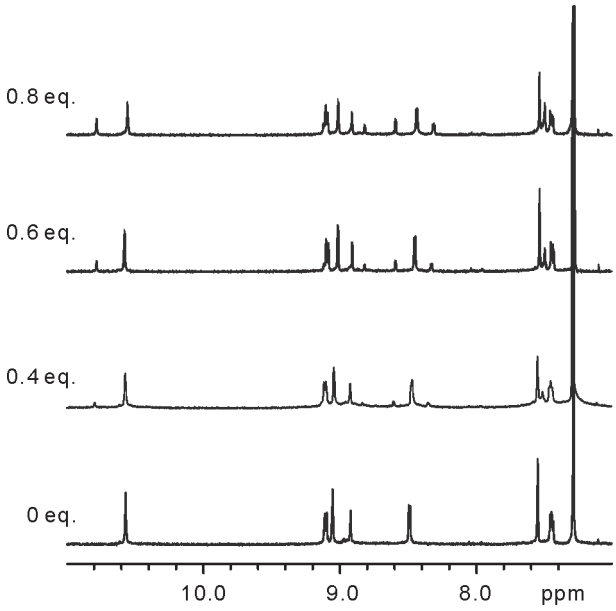

Figure S14. ^{1}H NMR titration of $B_{12}F_{12}^{2-}$ anion into a solution of **1**•$(BF_4)_4$ (0.25 mM) in $CDCl_3$:CD_3CN = 10:1 at 278 K.

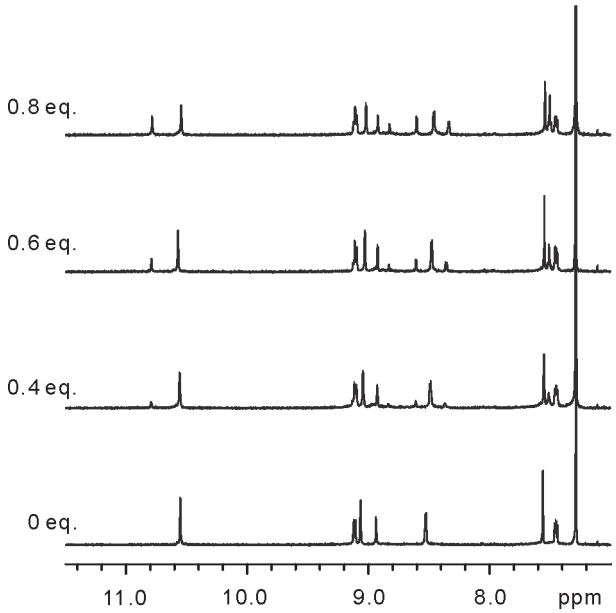

Figure S15. ^{1}H NMR titration of $B_{12}F_{12}^{2-}$ anion into a solution of **1**•$(BF_4)_4$ (0.25 mM) in $CDCl_3$:CD_3CN = 10:1 at 288 K.

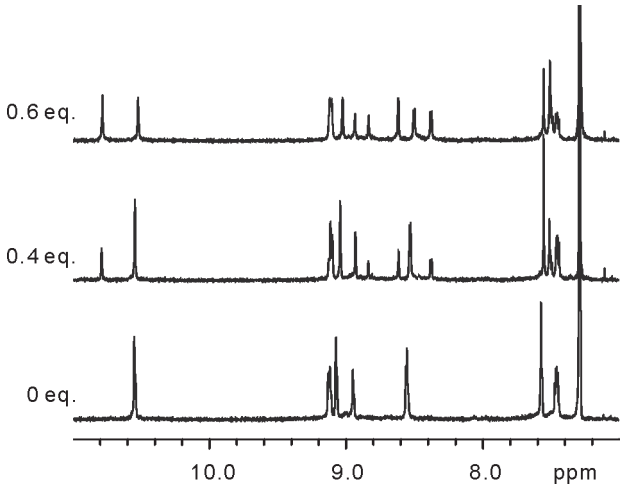

Figure S16. ^{1}H NMR titration of $B_{12}F_{12}^{2-}$ anion into a solution of **1**•$(BF_4)_4$ (0.25 mM) in $CDCl_3$:CD_3CN = 10:1 at 308 K.

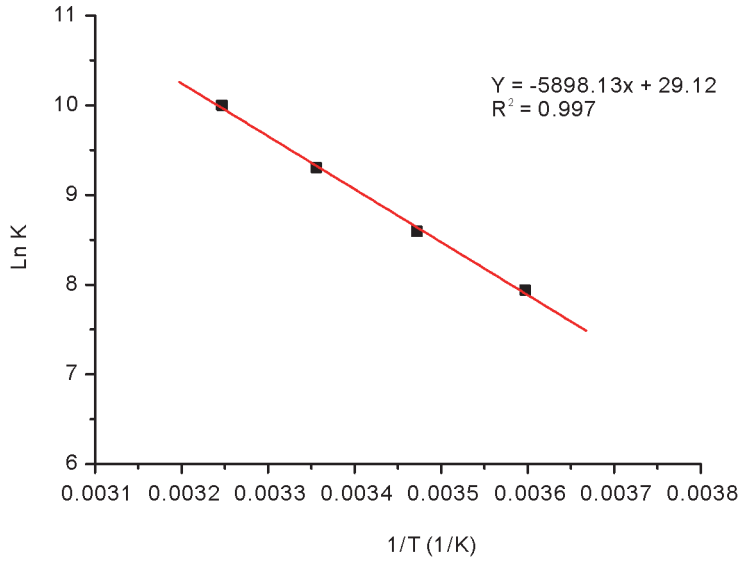

Figure S17. Van 't Hoff plot analysis of the association of host-guest complex **2** in $CDCl_3$:CD_3CN = 10:1. Experimental data were fitted to the Van 't Hoff equation using linear regression analysis (red line, R^2 = 0.997). ΔH and ΔS were determined to be 49.0 KJ mol^{-1} and 242.1 J mol^{-1} K^{-1}, respectively.

3 X-Ray Crystallography

Yellow crystals of **1**•$(NO_3)_4$-D_4 and **1**•$(NO_3)_4$-C_{4h} suitable for X-ray analysis were obtained upon slow diffusion of diethyl ether into a chloroform/acetonitrile/DMSO mixed solution of **1**•$(NO_3)_4$. Yellow crystals of **1**•$(BF_4)_4$-C_{4h} were obtained upon slow diffusion of diethyl ether into a chloroform/acetonitrile mixed solution of **1**•$(BF_4)_4$. Single crystals of complex **2** suitable for X-ray diffraction analysis were obtained by slow diffusion of diethyl ether into a chloroform/acetonitrile mixed solution of **1**•$(BF_4)_4$ and one point five equivalents equivalent of $K_2B_{12}F_{12}$.

Crystallographic data for compounds **1**•$(NO_3)_4$-D_4, **1**•$(NO_3)_4$-C_{4h}, and **1**•$(BF_4)_4$-C_{4h} were collected at the the Analysis and Testing Center in Huazhong University of Science and Technology (HUST) on a Rigaku MM007 HF rotating anode (0.8 kW). Compound **2** were collected ona Bruker Kappa Apex DUO diffractometer from Wuhan University. All data were diffracted at the CuKα wavelength, and data-collection strategies were based on Omega scans at 100(2) K. The Rigaku CrystalClear suite versions 1.36 and 2.1 were used to index, integrate and scale the data with a multi-scan absorption correction.

Data integration and reduction were undertaken with SAINT and XPREP[S3] or CrystalClear[S4]. Subsequent computations were carried out using the WinGX-32 graphical user interface[S5]. Structures were solved by intrinsic phasing algorithm implemented in SHELXT[S6] and then were refined with SHELXL[S7].The positions of the H atoms were deduced from coordinates of the non-H atoms. The non-H atoms were refined with anisotropic temperature parameters. H atoms were included for structure factor calculations but not refined. The SQUEEZE procedure[S8] implemented in WinGX was used in order to treat the regions with highly disordered solvent molecules (mainly chloroform, water, and dibutyl ether). SHELX ISOR and DELU restraints were used in the refinement strategy in order to reduce the anisotropic displacement parameters of the lateral chains. DFIX instructions were used to geometrically restraint most of these side chains. Crystallographic data along with specific details pertaining to the refinement (inclusively addressing CheckCIF alerts) follow. Crystallographic data have been deposited with the CCDC, under deposition numbers CCDC 1858187, compound **1**•$(NO_3)_4$-D_4; CCDC 1858188, compound **1**•$(NO_3)_4$-C_{4h}; CCDC 1858189, compound **1**•$(BF_4)_4$-C_{4h}; CCDC 1858190, compound **2**.

The final cif files were checked by IUCR's checkcif. The crystals employed in this study proved to be weakly diffracting and rapidly suffered solvent loss. Due to the characteristics mentioned above (large volume fractions of disordered solvent molecules and isobutyl side chains, weak diffraction intensity and moderate resolution), a number of A - level and B - level alerts remain in the check cif file. These

alerts are explicitly listed below and have been divided into two groups. They illustrate the limited practicality of the checkcif tool for medium size molecule crystallography.

GROUP 1 ALERTS

Alert level A

PLAT602_ALERT_2_A VERY LARGE Solvent Accessible VOID(S) in Structure ! Info

Alert level B

PLAT049_ALERT_1_B Calculated Density Less Than 1.0 gcm^{-3}

There is a significant amount of void volume in the lattice containing smeared electron density from disordered solvent and anions. The diffuse electron density could not be adequately modelled despite numerous attempts and the SQUEEZE function of PLATON[S8] was employed to remove the contribution of electron density associated with these disordered anions and solvent molecules. All these alerts are due to the squeeze procedure.

GROUP 2 ALERTS

Alert level A

SHFSU01_ALERT_2_A The absolute value of parameter shift to su ratio > 0.20

PLAT080_ALERT_2_A Maximum Shift/Error ..... 2.37 Why ?

Alert level B

THETM01_ALERT_3_B The value of sine(theta_max)/wavelength is less than 0.575

All these alerts in fact point to the same and unique problem which is the overall weak quality of the data and refinement statistics if compared to that expected for small molecule structures from highly diffracting.There is a significant amount of thermal motion in the extremities of the molecule and extensive thermal parameter and bond length restraints were required to facilitate realistic modelling for the organic parts of the structure. Reflecting the poor diffraction properties there is significant disorder present in the structure.Two isobutyl side chains were modelled as disordered with bond length and thermal parameter restraints applied to the disordered atoms to ensure a reasonable refinement .

Due to the problems described above, checkCIF gives these alerts. All of alerts (both A and B level) result from the poor diffraction properties (high residuals, low resolution, low bond precision, isotropic modelling of disordered atoms), large amount of thermal motion (high/low Ueqs and ratios, Hirshfeld differences, short contacts), and the use of SQUEEZE (discrepancy between given and expected molecular weights).

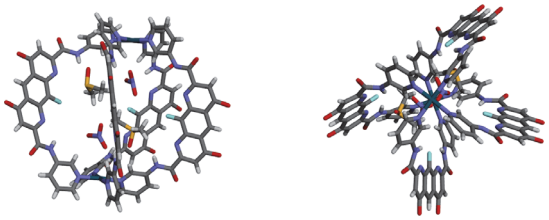

Figure S18. Side and top views of the crystal structure of **1**•$(NO_3)_4$-D_4. Anions are shown as CPK representations. Isobutyl side chains and disorder have been omitted for clarity.

Table S1: Crystal data and structure refinement for double helix **1**•$(NO_3)_4$-D_4

Formula	$C_{132}\,H_{136}\,F_4\,N_{26}\,O_{24}\,Pd_2\,S_2$
M	2823.58
Crystal system	orthorhombic
Space group	Pbcm
a/Å	21.3685(3)
b/Å	26.9448(4)
c/Å	41.0041(8)
α/°	90
β/°	90
γ/°	90
V/Å^3	23608.9(7)
T /K	100.00(10)
Z	4
ρ/g cm^{-1}	0.794
size (mm)	0.2×0.2×0.2
λ/ Å	1.54184
μ/mm^{-1}	1.797
Independent reflections	23740
measured reflections	109782
parameters/restraints	866/17
*R*1, *wR*2	0.0794，0.2359
goodness of fit	0.926

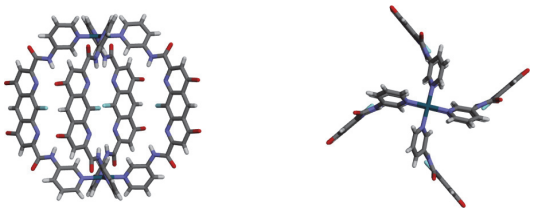

Figure S19. Side and top views of the crystal structure of **1**•$(NO_3)_4$-C_{4h}. Isobutyl side chains and disorder have been omitted for clarity.

Table S2: Crystal data and structure refinement for **1**•$(NO_3)_4$-C_{4h}

Formula	$C_{128}\ H_{124}\ F_4\ N_{24}\ O_{16}\ Pd_2$
M	2543.30
Crystal system	tetragonal
Space group	I4/m
a/Å	18.9268(6)
b/Å	18.9268(6)
c/Å	24.7717(9)
α/°	90
β/°	90
γ/°	90
V/Å^3	8873.8(6)
T /K	100.01(13)
Z	2
ρ/g cm^{-1}	0.952
size (mm)	0.1×0.2×0.2
λ/ Å	1.54184
μ/mm^{-1}	2.096
Independent reflections	4489
measured reflections	15667
parameters/restraints	204/0
*R*1, *wR*2	0.0692，0.1820
goodness of fit	0.937

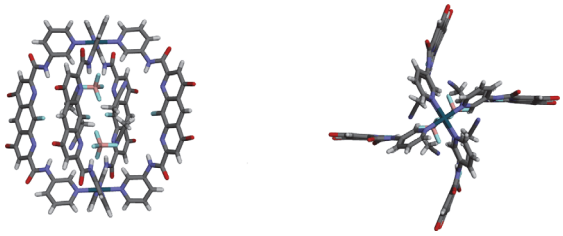

Figure S20. Side and top views of the crystal structure of **1**•$(BF_4)_4$-C_{4h}. Anions are shown as CPK representations. Isobutyl side chains and disorder have been omitted for clarity.

Table S3: Crystal data and structure refinement for **1**•$(BF_4)_4$-C_{4h}

Formula	$C_{136}\,H_{136}\,B_4\,F_{20}\,N_{28}\,O_{16}\,Pd_2$
M	3054.81
Crystal system	triclinic
Space group	$P\bar{1}$
a/Å	17.0266(2)
b/Å	17.8919(5)
c/Å	18.1716(6)
α/°	74.712(10)
β/°	66.581(8)
γ/°	78.682(9)
V/Å^3	4873.8(4)
T /K	100
Z	1
ρ/g cm^{-1}	1.041
size (mm)	0.2×0.2×0.2
λ/ Å	1.54178
μ/mm^{-1}	2.104
Independent reflections	16426
measured reflections	16426
parameters/restraints	938/0
*R*1, *wR*2	0.0879，0.2279
goodness of fit	1.005

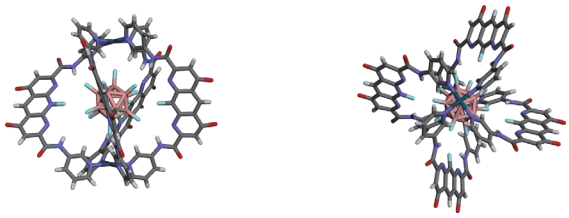

Figure S21. Side and top views of the crystal structure of **2**. Anions are shown as CPK representations. Isobutyl side chains and disorder have been omitted for clarity.

Table S4: Crystal data and structure refinement for **2**

Formula	$C_{128}\,H_{124}\,B_{14}\,F_{24}\,N_{24}\,O_{16}\,Pd_2$
M	3074.64
Crystal system	monoclinic
Space group	P21/n
a/Å	19.8811(9)
b/Å	22.8682(11)
c/Å	44.582(2)
α/°	90
β/°	94.821(3)
γ/°	90
V/Å^3	20197.2(17)
T /K	100(2)
Z	4
ρ/g cm^{-1}	1.011
size (mm)	0.1×0.2×0.2
λ/ Å	1.54178
μ/mm^{-1}	2.051
Independent reflections	29134
measured reflections	189676
parameters/restraints	1889/85
*R*1, *wR*2	0.1030，0.2969
goodness of fit	1.147

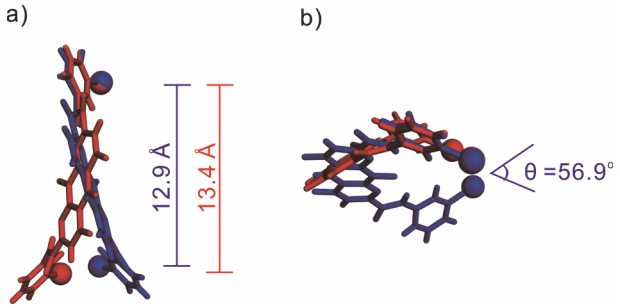

Figure S22. Front (a) and top (b) views of partial overlay of sub-structures of **1**•$(NO_3)_4$-D_4 (blue), and **1**•$(NO_3)_4$-C_{4h} (red) revealing the relationship between the twisting in the ligand structures, the azimuthal angles for coordination, and Pd^{II}/Pd^{II} distances.

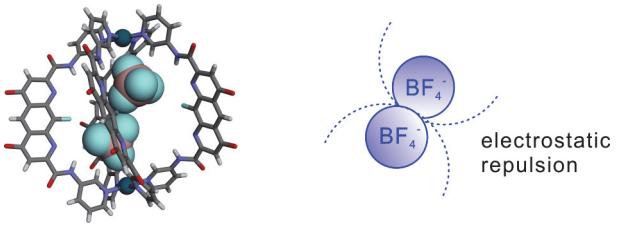

Figure S23. Structural imitation of **1**•$(NO_3)_4$-D_4 with two tetrafluoroborate instead of two nitrate anions inside. The fake structure indicated these two encapsulated tetrafluoroborate anions would be sterically confined and generate electrostatic repulsion. The fake structure was fabricated based on the crystal structures of **1**•$(NO_3)_4$-D_4 and **1**•$(NO_3)_4$-C_{4h}, wherein the relative positions and orientations between the tetrafluoroborate anions and Pd^{II} ions were restricted (distances $d_{Pd\cdots B}$ = 4.24 Å and angles $\angle_{Pd\cdots\ Pd\cdots\ B}$ = 17.6° were fixed, and one fluorine atom of each tetrafluoroborate was restricted towards Pd^{II}).

4 Circular dichroism studies

Solutions of helicates **1**•$(NO_3)_4$ and **1**•$(BF_4)_4$ were prepared in 10:1 (v/v) $CDCl_3/CD_3CN$ and measured by ^{1}H NMR (500 µM) and CD (50 µM) spectroscopy. ^{1}H NMR and CD spectra of these samples were further recorded after addition of 4 equivalents of [nBu_4N][Δ-TRISPHAT] anions to these solutions.

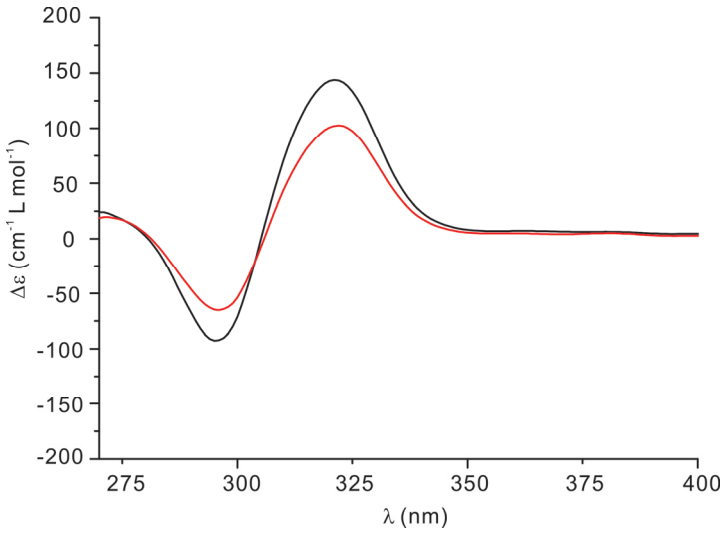

Figure S24. CD spectra ($CDCl_3$:CD_3CN = 10:1, 50 µM) of helicates **1**•$(NO_3)_4$ (red line) and **1**•$(BF_4)_4$ (black line) in the presence of 4 equiv. of Δ-TRISPHAT anions. Contributions from TRISPHAT anions were subtracted.

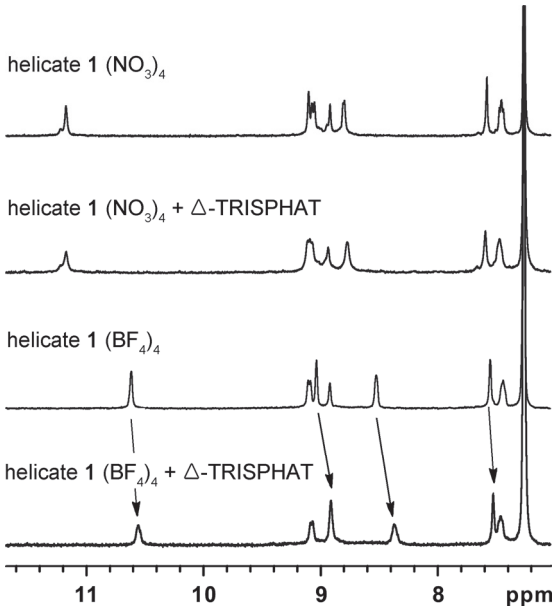

Figure S25. ^{1}H NMR spectra ($CDCl_3$:CD_3CN = 10:1, 0.5 mM) of helicates **1**•$(NO_3)_4$ and **1**•$(BF_4)_4$, and their solutions in the presence of 4 equiv. of Δ-TRISPHAT anions.

5 Volume calculations

In order to determine the available void volume within helicates **1**•$(NO_3)_4$-D_4 and **1**•$(NO_3)_4$-C_{4h}, VOIDOO calculations[S9] based on the crystal structures were performed. The standard parameters tabulated below were used.

Probe radius (set by default, water-sized)	1.4
Maximum number of volume-refinement cycles	30
Minimum size of secondary grid	3
Grid for plot files	0.2
Primary grid spacing	0.1

A pocket of 311 Å^3 in volume was observed within the crystal structure of **1**•$(NO_3)_4$-D_4 and of 367 Å^3 within the crystal structure of **1**•$(NO_3)_4$-C_{4h} (see Figure S24).

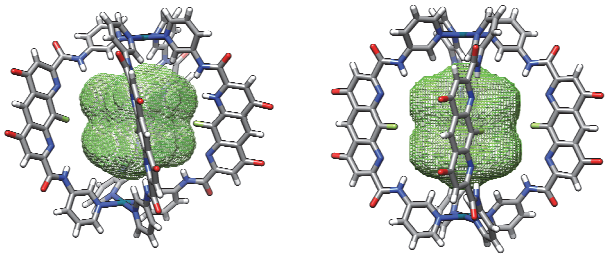

Figure S26. VOIDOO-calculated void space as shown (green mesh) within the crystal structure of **1**•$(NO_3)_4$-D_4 (left) and **1**•$(NO_3)_4$-C_{4h} (right).

6 NMR spectra

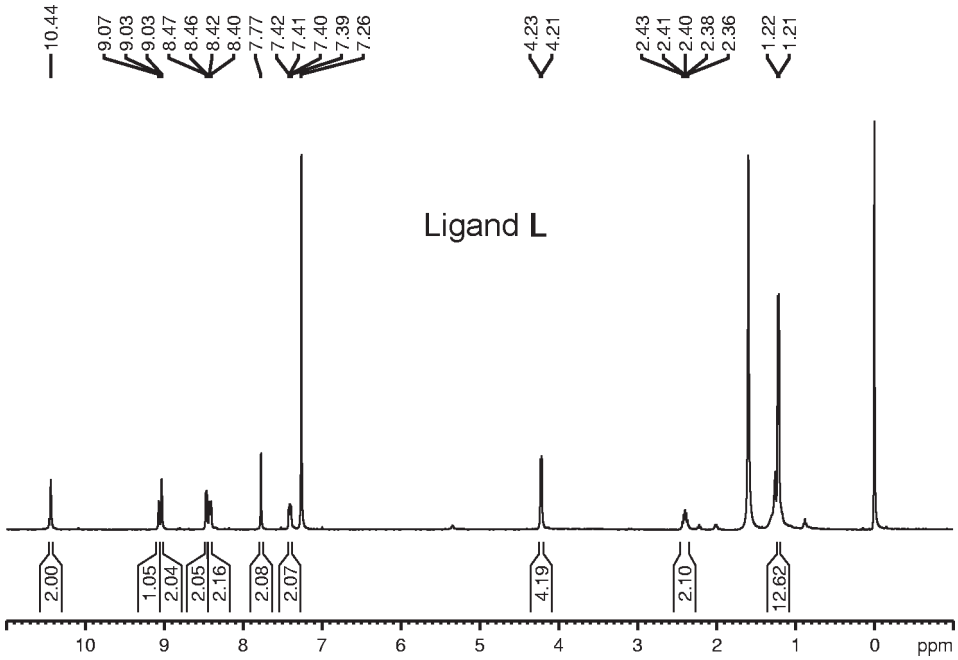

Figure S27. ^{1}H NMR spectrum (400 MHz) of ligand **L** in $CDCl_3$.

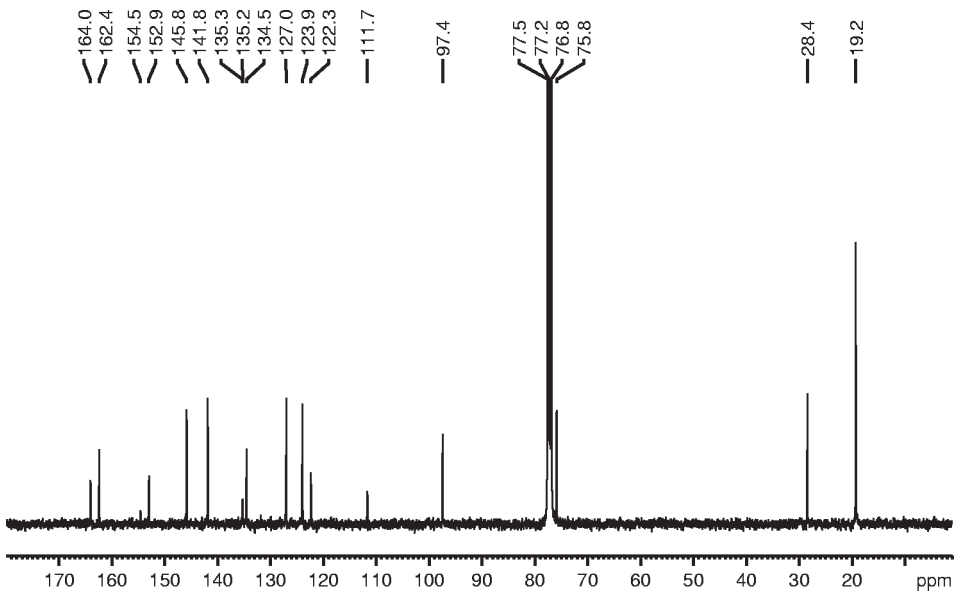

Figure S28. ^{13}C NMR spectrum (100 MHz) of ligand **L** in $CDCl_3$.

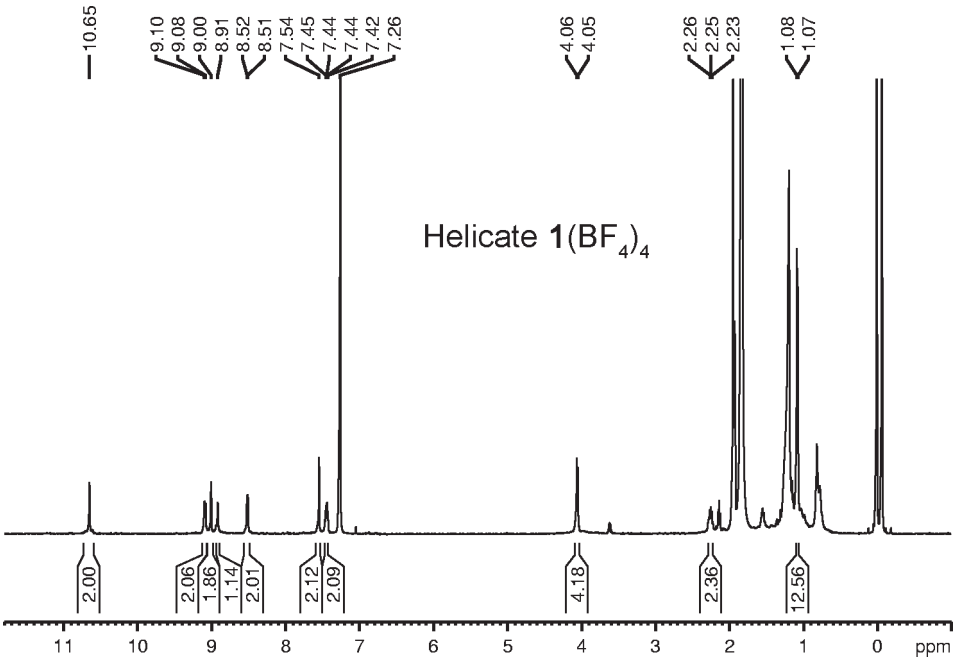

Figure S29. ^{1}H NMR spectrum (400 MHz) of helicate **1**•$(BF_4)_4$ in $CDCl_3$/ CD_3CN (10:1 vol/vol).

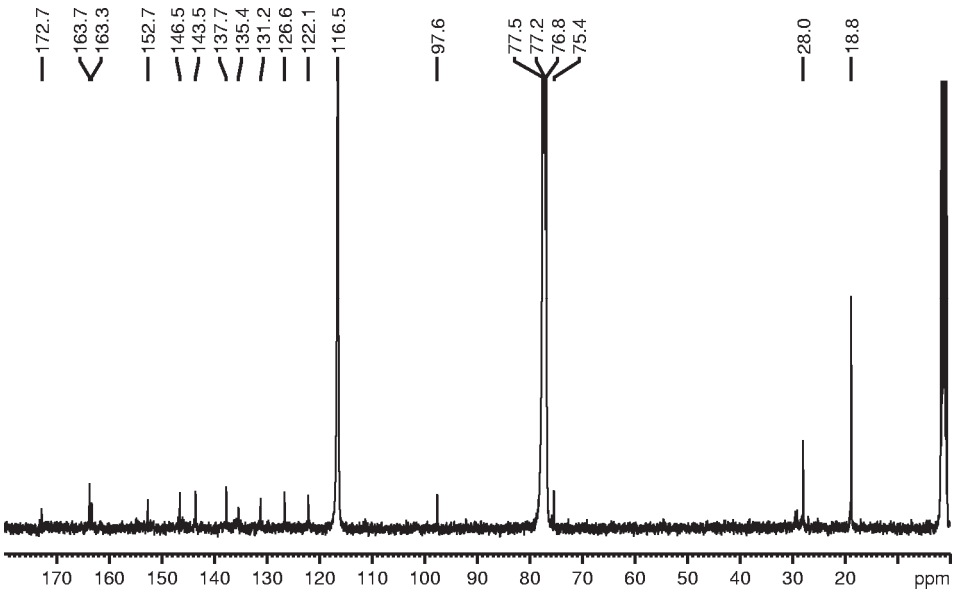

Figure S30. ^{13}C NMR spectrum (100 MHz) of helicate **1**•$(BF_4)_4$ in $CDCl_3$/ CD_3CN (10:1 vol/vol).

7 References

(S1) Fulmer, G. R.; Miller, A. J.; Sherden, N. H.; Gottlieb, H. E.; Nudelman, A.; Stoltz, B. M.; Bercaw, J. E.; Goldberg, K. I. *Organometallics* **2010**, *29*, 2176–2179.

(S2) Bao, C.; Kauffmann, B.; Gan, Q.; Srinivas, K.; Jiang, H.; Huc I. *Angew. Chem. Int. Ed.* **2008**, *47*, 4153–4156.

(S3) Bruker-Nonius, *APEX, SAINT and XPREP*, Bruker AXS Inc., Madison, Wisconsin, USA, **2013**.

(S4) CrystalClear v. 2.0 ed., Rigaku Americas and Rigaku Corporation., 9009 TX, USA **1997-2009**.

(S5) Farrugia, L. J. *J. Appl. Crystallogr.* **1999**, *32*, 837–837.

(S6) Sheldrick, G. M. Acta Crystallogr. Sect. **2015**, *A71*, 3–8.

(S7) Sheldrick, G. *Acta Cryst.* **2008**, *A64*, 112–122.

(S8) van der Sluis, P.; Spek, A. L. *Acta Cryst.* **1990**, *A46*, 194–201.

(S9) Kleywegt, G. J.; Jones, T. A. *Acta Cryst.* **1994**, D*50*, 178–185